

Order-by-disorder in the antiferromagnetic Ising model on an elastic triangular lattice

Yair Shokef^{*}, Anton Souslov[†] and Tom C. Lubensky[†]

^{*}Department of Materials and Interfaces, Weizmann Institute of Science, Rehovot 76100, Israel, and [†]Department of Physics and Astronomy, University of Pennsylvania, Philadelphia, PA 19104, USA

Submitted to Proceedings of the National Academy of Sciences of the United States of America

Geometrically frustrated materials have a ground-state degeneracy that may be lifted by subtle effects, such as higher order interactions causing small energetic preferences for ordered structures. Alternatively, ordering may result from entropic differences between configurations in an effect termed order-by-disorder. Motivated by recent experiments in a frustrated colloidal system in which ordering is suspected to result from entropy, we consider in this paper the antiferromagnetic Ising model on a deformable triangular lattice. We calculate the displacements exactly at the microscopic level, and contrary to previous studies, find a partially disordered ground state of randomly zigzagging stripes. Each such configuration is deformed differently and thus has a unique phonon spectrum with distinct entropy, lifting the degeneracy at finite temperature. Nonetheless, due to the free-energy barriers between the ground-state configurations, the system falls into a disordered glassy state.

geometric frustration | order by disorder | magnetoelasticity | colloidal monolayer

Abbreviations: FCC, face-centered-cubic; HCP, hexagonal-close-packing

Frustrated systems are characterized by interactions that may not be satisfied simultaneously [1]. This leads to a degenerate and thus disordered ground state, and naively one would expect to have disorder down to zero temperature [2]. However, the frustrated phase is very sensitive to small perturbations that can order it. These include anisotropic [3] or longer-range [4] interactions and lattice deformations [5, 6, 7, 8, 9, 10] as well as entropic effects that may lift the ground-state degeneracy at finite temperature, in a process termed order-by-disorder [11, 12, 13, 14, 15, 16]. Frustration and its relief due to order-by-disorder are traditionally investigated in antiferromagnets and, in particular, in compounds that have a triangular lattice structure [17, 18, 19, 20]. Recent experiments have demonstrated that artificial systems made of mesoscopic building blocks such as single-domain magnetic islands [21] or colloidal spheres [22] exhibit behavior which is similar to that of magnetic systems comprised of atomic-scale particles. Such mesoscopic systems enable direct visualization of the dynamics at the single-particle level and thus provide insight into the microscopic physical mechanisms responsible for the peculiar properties of frustrated matter. In this paper we address the theoretical underpinnings of these new experimental systems and thus provide a vital step in understanding their unusual behavior and its connection to atomic-scale antiferromagnets.

A densely-packed monolayer of hard spheres buckles out of its plane when it is confined between walls that are separated by slightly more than a single sphere diameter [23]. Entropic forces depending only on geometry give rise to effective anti-ferromagnetic interactions favoring motion of neighboring spheres toward opposite walls [24], leading at high densities to stripes of alternating up and down spheres. The close-packed state is highly degenerate: the same maximal density is obtained by straight stripes or by any set of parallel stripes that zigzag within the hexagonally-packed layer [22, 24, 25, 26, 27, 28]. Recent experiments indicate a

possible preference of the stripes to be straight rather than to zigzag randomly in the plane, suggesting that at densities below close-packing there is an order-by-disorder effect giving an entropic advantage for straight stripes [22].

This quasi-two-dimensional problem is strongly related to the old, yet unsolved question of what is the stable high-density structure of hard spheres, face-centered-cubic (FCC) or hexagonal-close-packing (HCP) [29, 30, 31]. In three dimensions, maximal density is obtained by stacking hexagonally packed layers with arbitrary sideways shifts between the close-packed positions. And, as for the buckled monolayer, slightly below close-packing it is not clear which structure has the greatest entropy. Experiments on colloidal crystals that were grown slowly enough exhibit FCC order [32], while there is controversy on whether the theoretical estimates have reached the accuracy required to resolve the elusive entropic difference between FCC and HCP [33, 34, 35, 36, 37, 38].

As for the FCC *vs* HCP question, the entropy, or free volume, of buckled hard spheres is a collective function of the positions of all particles, thus the ability to obtain analytical results for it is very limited. Thus, instead of *approximating* the entropy of this hard-sphere system, we consider the anti-ferromagnetic Ising model on a deformable triangular lattice. This model has the same degenerate ground state of zigzagging stripes as the colloidal system, and for it we can *exactly* calculate the free-energy difference between the competing configurations. We find that straight stripes are always favored entropically. However, the free-energy barriers between various ground states are huge compared to this entropic gain, causing the system to fall into a disordered glassy state upon cooling.

In our Ising model, each site i at continuous position \vec{r}_i on a triangular network is occupied by a particle of discrete spin $\sigma_i = \pm 1$, and each nearest neighbor bond comprises a harmonic spring of stiffness K and relaxed length a , see Fig. 1A. The internal energy of the system depends only on the spin product $\sigma_i \sigma_j$ of neighboring particles and on their relative positions, $\delta r_{ij} = |\vec{r}_i - \vec{r}_j| - a$. The model's Hamiltonian is given by the following sum over all nearest-neighbor pairs $\langle ij \rangle$,

$$\mathcal{H} = \sum_{\langle ij \rangle} \left[(1 - \epsilon \delta r_{ij}) J \sigma_i \sigma_j + \frac{K}{2} \delta r_{ij}^2 \right]. \quad [1]$$

Reserved for Publication Footnotes

The antiferromagnetic interaction strength is equal to $J > 0$ for particles separated by the relaxed spring length a , and decreases linearly with distance at a rate $\epsilon > 0$. This mimics the buckled colloidal monolayer in the following way: For hard spheres, free energy is determined by their free volume. However, it is convenient to reduce this to an effective two-particle repulsive interaction. While the particles are confined to be quasi-two-dimensional, they do have a limited freedom to move in the vertical direction, and thus nearest neighbors prefer to sit at opposite heights. We can now map the vertical position of each particle onto an Ising degree of freedom, due to a preference for either an “up” or “down” state. This leads to an effective two-dimensional antiferromagnetic Ising model, with the coupling between the elastic and the magnetic degrees of freedom as reflected in our Hamiltonian (1), i.e. the effective antiferromagnetic interaction decays as the in-plane separation increases [24].

We model the in-plane entropic repulsion between neighboring spheres by a rotationally invariant central-force harmonic spring [Eq. (1)]. Approximate versions of this model have been studied previously: Ref. [6] uses a linearized long-wavelength elastic energy, invariant with respect to only infinitesimal rotations, that limits deformations to be small and to vary slowly in space, while in Ref. [5] deformations are taken to be uniform.

In this paper we present results for the case in which the total area of the system is fixed to the area of a triangular lattice with lattice constant equal to a . However, we obtained qualitatively similar results for systems compressed or dilated with respect to this simple situation. From the equivalence between ensembles we thus expect to get the same results also when considering the fixed pressure case, which is probably more appropriate for the colloidal experiments.

As in the rigid triangular-lattice model [2, 3], the antiferromagnetic interactions along each three-particle loop in our deformable network cannot be satisfied simultaneously, and energy is minimized by having two satisfied ($\sigma_i \sigma_j = -1$) bonds and a single frustrated ($\sigma_i \sigma_j = 1$) bond around each triangular plaquette. Because of the magnetoelastic coupling, energy may be lowered by stretching the frustrated bonds by a factor f and compressing the satisfied ones by a factor s . We fix the area of each resulting isosceles triangle to be that of the initial equilateral plaquette with sides a , and thus we can parametrize the deformation by the head angle β (see Fig. 1B, inset): $f(\beta) = 3^{1/4}(\tan \frac{\beta}{2})^{1/2}$, $s(\beta) = 3^{1/4}(2 \sin \beta)^{-1/2}$. Minimizing the energy (1) with respect to β yields (see SI Appendix)

$$(2s' - f')J\epsilon + [2(s - 1)s' + (f - 1)f']Ka = 0. \quad [2]$$

Figure 1B shows how the triangles deform from $\beta = 60^\circ$ toward $\beta = 180^\circ$ as the ratio $b \equiv \frac{J\epsilon}{Ka}$ of the magnetoelastic interaction strength to the lattice rigidity grows.

Thus, each plaquette of the triangular lattice would minimize its energy by deforming into an isosceles triangle. We now show how this can be accommodated in the ground state by global deformations of the system. In the rigid triangular lattice, since each triangle must have exactly one frustrated bond, five nearest-neighbor configurations are allowed in the ground state (Fig. 1C) [39]. Requiring that the angle opposing each frustrated bond deforms to $\beta > 60^\circ$ selects configurations (iii) and (iv) [22, 24], which give rise to zigzagging stripes. Thus, selecting a stripe of frustrated bonds defines a ground state of the lattice. It can be constructed by starting with a row of alternating spins (along the horizontal axis) and stacking copies of this row (along the vertical axis), as shown in Fig. 2. The intra-row and inter-row separations are sa and

$sa \sin \beta$, respectively, and the lateral shifts are determined by the arbitrary polarity of each row with respect to the one preceding it. Since these rows of alternating spins may be in any of the three principal directions of the network, and for a system of N particles, each of the \sqrt{N} rows may be in one of two states, the ground-state degeneracy is $3 \cdot 2^{\sqrt{N}}$.

This partially-disordered ground state is realized by deformations that may vary rapidly in space; if deformations are assumed to be homogeneous [5] or to vary slowly [6], straight stripes are selected. In particular, the zigzagging stripes that minimize our microscopic Hamiltonian (1) have a higher energy than straight stripes in the coarse-grained Hamiltonian considered in [6]. The ground state of zigzagging stripes that we find here is precisely the state that maximizes the packing density of buckled spheres [22, 24], which constitutes the connection of our model to the colloidal system.

Given the high ground-state degeneracy and the fact that it takes a discrete energy (of order J) to flip a spin in the ground state, one might naively expect to find a stable phase of randomly zigzagging stripes at sufficiently low temperature ($k_B T \ll J$). However, at positive temperature, the entropy of particle fluctuations around the energy-minimizing position is different in the different ground-state configurations. We will show that the state with straight stripes has lower free energy (or greater entropy) than other states, making it the stable thermodynamic phase at arbitrarily low temperature. Nonetheless, the resulting free-energy differences between the different zigzagging realizations are much smaller than the free-energy barriers between the ground-state configurations and the system typically falls into disordered meta-stable configurations.

To demonstrate the peculiar slow dynamics of this model, we used Monte-Carlo simulations in which individual particles can flip their spin or move continuously in the plane and in which the simulation box may change its shape to accommodate the global deformations of the network [24]. We start from a disordered state at high temperature, and we slowly cool the system at a rate r (time is measured in attempted Monte-Carlo steps per particle). Figure 3A shows that at high temperature the system follows an equilibrium curve irrespective of cooling rate, while below a certain temperature ($T \approx 0.6$ for the parameter values shown here), the system's energy has a clear cooling rate dependence. Apparently, if the cooling is slow enough ($r \leq 10^{-6}$ here), the system manages to reach the ground state.

Figure 4A shows that indeed if the system is cooled too rapidly ($r = 10^{-4}$) it falls into a disordered state with multiple small domains of a local stripy structure. For a slower cooling rate ($r = 10^{-6}$, Fig. 4B), the system finds a ground-state configuration with zigzagging stripes, such that the local configurations (iii) and (iv) defined in Fig. 1C are roughly equally represented, thus corroborating this phase as randomly zigzagging stripes. Figure 4C shows that for even slower cooling ($r = 10^{-8}$), there is preference for ground-state configurations in which the stripes are more straight than bent, namely configuration (iii) is preferred over (iv). This is quantified in Fig. 3, B, C, which shows results obtained by averaging over multiple realizations for each system size and cooling rate. For very fast cooling, the system remains quite disordered with $P(iii)/P(iv) \approx 0.5$, in accordance with the combinatoric weights of these two local configurations. For $r \leq 10^{-6}$, the system manages to find its ground state, as seen by the fact that $P(iii) + P(iv) = 1$, namely all particles are in one of these two states. For $r = 10^{-6}$ these two states are equally probable, $P(iii) \approx P(iv)$, as one would expect for randomly zigzagging stripes. However, as the cooling rate is decreased even more, there is a clear preference for the straight

configuration (*iii*) over the bent one (*iv*). This is in qualitative agreement with recent experiments [40] exploring the cooling rate dependence of our colloidal antiferromagnet [22].

Although the Ising degrees of freedom in our model do not have natural physical dynamics associated with them, the Monte-Carlo dynamics we employ are useful in exploring actual out-of-equilibrium dynamics of spin systems [41, 42, 43, 44]. Thus, to our understanding, the cooling rate in our simulations should be interpreted as being directly proportional to the experimental cooling rate, and it would be interesting to explore the connection between the transition rates we apply in our Monte-Carlo scheme and the actual physical quantities in the experiments.

The preference we observe for straight over bent stripes comes from an entropic difference between the two, as is explained in the following low-temperature expansion. Expanding the Hamiltonian about the fixed-spin ground state to lowest order, we find terms quadratic in particle displacements. Thus, the lowest-energy excitations are harmonic modes of vibrations with frequencies which we denote by $\{\omega_k\}$ (note that k indexes the normal modes and does not necessarily refer to a wavevector). We assume the temperature is low enough ($k_B T \ll J$) to ignore spin flips, yet high enough ($k_B T \gg \hbar\omega$) to ignore quantum effects. Therefore, we use the canonical partition function of a classical harmonic oscillator of frequency ω , $Z \propto k_B T / \omega$, to write the free energy of the system as the following sum over all normal modes

$$\mathcal{F} = -k_B T \log Z = -k_B T \left[\sum_k \log \left(\frac{k_B T}{\omega_k} \right) + \text{const.} \right] \quad [3]$$

We emphasize at this point that the frequencies $\{\omega_k\}$ refer to the fast oscillations of the positional degrees of freedom, which at low enough temperature are expected to be much faster than the spin flips.

The different spin states $\{\sigma_i\}$ of the various ground-state configurations impose different deformations $\{\vec{r}_i\}$, thus each one has a distinct spectrum $\{\omega_k\}$ of eigen-frequencies, and a different entropy, which is expressed as a different temperature dependence of the free energy \mathcal{F} in Eq. (3). At $T = 0$, entropy is irrelevant and all ground-state configurations are equivalent, but at $T > 0$ this degeneracy is lifted and the configuration with the minimal free energy is selected. The frequencies of all vibrational modes scale as $\omega_k^2 \propto K/M$, where M is the mass of each particle. The normalized spectrum depends on the spin state $\{\sigma_i\}$ and on the deformation angle β , which is set by $b \equiv \frac{J\epsilon}{K\alpha}$ (see Eq. (2) and Fig. 1B). Hence we define

$$\mathcal{A}(\{\sigma_i\}, \beta) \equiv \frac{1}{N} \sum_k \log \left(\sqrt{\frac{M}{K}} \omega_k \right), \quad [4]$$

and write $\mathcal{F} = N k_B T [\mathcal{A}(\{\sigma_i\}, \beta) + \text{const.}]$. Thus minimizing \mathcal{F} is equivalent to minimizing \mathcal{A} .

We can analytically calculate the normal modes of vibrations of the deformed lattice for any ground state with a periodic repetition of straight (*iii*) and bent (*iv*) segments (see SI Appendix). In such cases the normal modes are phonons and the index k labeling them may be associated with their wavevector. The free-energy coefficient, \mathcal{A} , may then be obtained by numerically summing over the appropriate Brillouin zone. Figure 2 highlights the unit cells in ground states with periods of one, two, and five particles. Now we consider ground states with larger unit cells, and show that the free energy is mainly determined by the fraction $p_s \equiv P(\text{iii})/[P(\text{iii}) + P(\text{iv})]$ of straight segments. To clarify which configurations we used in these calculations, we show in Fig. 5 several representative unit cells. For example,

$p_s = 1/3$ in a single configuration with three particles in its unit cell (Fig. 5A), but also in two configurations with six particles (Fig. 5B), in six with nine particles (Fig. 5C), and in an increasing number of other configurations with larger unit cells. Similarly, for $p_s = 1/2$, we show the two configurations with four particles per unit cell in Fig. 5D and the six with eight particles in Fig. 5E.

Figure 6A-C shows the results obtained by numerically evaluating Eq. (4) for ground states with unit cells consisting of up to 13 particles, plotted vs p_s (see SI Appendix for more details and Tables S4-S5 for the entire data plotted). We find that the free energy is bounded between the extreme cases of straight stripes ($p_s = 1$, Fig. 2A) and bent stripes ($p_s = 0$, Fig. 2B). Moreover, the approximate collapse of the results for all calculated unit cells to a single curve provides strong support for the hypothesis that only the ratio between straight and bent segments is important and not the order in which they are positioned or the period of the pattern they form. Finally, the roughly linear dependence of \mathcal{A} on p_s indicates that the free energy may be approximated as a linear combination of contributions from the straight and bent segments. Since the ground state is determined by a one-dimensional sequence of straight and bent segments, this result implies that the system may be well approximated by an effective one-dimensional non-interacting Hamiltonian. For $\beta = 155^\circ$ (Fig. 6C) we observe substantial deviations from the prediction of such a non-interacting Hamiltonian. It would be interesting to understand whether these deviations result from our limited numerical accuracy in evaluating so small free-energy differences, or from additional considerations that affect the physics of this system at such large deformations.

In our elastic Ising model, the low-temperature free energy of in-plane positional fluctuations is determined by the dimensionless ratio $b \equiv \frac{J\epsilon}{K\alpha}$ between the magnetoelastic interaction strength to the lattice rigidity. This ratio sets the deformation angle β of each isosceles triangle in the ground-state (see Eq. (2) and Fig. 1B). In the corresponding system of buckled colloids, the deformation angle β of each isosceles plaquette in the close-packed state (which is equivalent to the Ising model's ground state), is similarly dictated by the ratio of each sphere's diameter to the separation between the confining walls [24]. We expect the colloidal system to exhibit a similar order-by-disorder effect that will be governed by the deformation angle β , and therefore we plot in Fig. 6D the free-energy difference $\mathcal{A}_0 - \mathcal{A}_1$ between straight and bent segments vs the geometrical parameter β rather than vs the physical parameter b .

For extremely rigid lattices that hardly deform ($\beta \approx 60^\circ$), straight and zigzagging stripes are almost equivalent in terms of their particle displacements and therefore $\mathcal{A}_0 \approx \mathcal{A}_1$. As β increases, straight stripes develop an entropic advantage which comes from the fact that the straight-stripe ground state is the most anisotropic and hence has the most nonuniform distribution of eigen-frequencies, and thus the maximal entropy [13]. For extremely large deformations ($\beta > 100^\circ$) we observe a decrease in $\mathcal{A}_0 - \mathcal{A}_1$ which reaches a minimal value at $\beta \approx 155^\circ$ and then increases again as $\beta \rightarrow 180^\circ$. In the SI Appendix we show how this non-monotonic behavior results from the numerical structure of the dispersion relations. In particular, we identify in Fig. S10 the region in reciprocal space which dominates the free-energy difference between straight and bent stripes. The magnitude of the free-energy difference in this region grows monotonically with β , however the size of this region decreases, which gives rise to the non-monotonic behavior seen in Fig. 6D for $60^\circ \leq \beta \leq 155^\circ$. For $\beta \geq 155^\circ$ the free-energy difference has a different wavevector dependence (see Fig. S10) which gives rise to the second increase

in the total free-energy difference at such large deformations. It would be interesting to theoretically understand the deeper origins and possible implications of this non-monotonic behavior. Note that for large values of β , the distance to some of the next-nearest neighbors becomes smaller than the distances between nearest neighbors. This introduces further complications beyond the analysis presented in this paper which assumes only nearest-neighbor interactions. Overall, our numerical results show that for all ground-state deformations, straight stripes are preferred entropically, however their entropic advantage is extremely small. We observed the same qualitative behavior when allowing the system's total volume to vary.

Before concluding we note that the free energy coefficient \mathcal{A} given in Eq. (4) and plotted in Fig. 6 is defined for each specific realization of the stripes. Randomly zigzagging stripes which mix straight and bent segments are highly degenerate, and their free energy possesses also a configurational entropy (or entropy of mixing) which competes with the vibrational entropic advantage of straight stripes that we found. However, due to the one-dimensional character of the ground state, this configurational entropy is sub-extensive in system size and scales as \sqrt{N} . The vibrational free energy of Eq. (4) enters as an extensive quantity which scales linearly with N in \mathcal{F} , and is thus dominant in the thermodynamic limit. As a result, straight stripes are favored. This may be the reason for the limited ability of our simulations to reach perfect straight stripes, and for the smaller values of $P(iii)/P(iv)$ for smaller systems in Fig. 3C. To test this, we repeated the simulations at parameter values where the difference in \mathcal{A} between straight stripes and zigzags is smaller and indeed found a weaker preference for straight stripes.

In summary, our exact microscopic description of this previously-studied [5, 6] elastic Ising model reveals a highly-degenerate, partially-disordered ground state. We find a much richer behavior since entropy lifts the degeneracy at any positive temperature. However, large free-energy barriers between the ground-state configurations induce a glassy phase of zigzagging stripes. Although equilibration is strongly hindered in this glassy phase, the straight-stripe structures obtained in it result from the minute entropic differences in the equilibrium free energies of the various stripe realizations. The fact that this model is amenable to analytic treatment makes it appealing as a prototypical model for studying such order-by-disorder phenomena in a broader context. Moreover, the current approach to experimentally studying frustration relief by lattice deformations in antiferromagnets is based on quite indirect measurements of lattice deformations [45, 46]. Our work makes direct contact to a colloidal system [22] in which frustration and its relief are governed by similar physical mechanisms, yet it has the advantage that local deformations can be directly measured in it. Interestingly, several recent experimental works are focused on measuring the normal modes of vibration in colloidal systems [47, 48, 49, 50]. On top of understanding deformable antiferromagnets and mesoscopic model systems for them, we expect that results obtained for our system will shed light on questions such as the statistical mechanics of sphere packings and the physical origins of glassy dynamics.

ACKNOWLEDGMENTS.

We thank Ehud Altman, Assa Auerbach, Bulbul Chakraborty, John Chalker, Kedar Damle, Chris Henley, Randy Kamien, Amit Keren, Joel Lebowitz, Roderich Moessner, Ido Regev, Per Rikvold, and Peter Yunker for helpful discussions. This work is supported by NSF MRSEC Grant No. DMR-0520020.

- Moessner R, Ramirez AR (2006) Geometrical frustration. *Phys. Today* 59:2426.
- Wannier GH, (1950) Antiferromagnetism. The triangular Ising net. *Phys. Rev.* 79:357364.
- Houtappel RMF (1950) Order-disorder in hexagonal lattices. *Physica* 16:425-455.
- Metcalf BD (1974) Ground state spin orderings of the triangular Ising model with the nearest and next nearest neighbor interaction. *Phys. Lett. A* 46:325-326.
- Chen ZY, Kardar M (1986) Elastic antiferromagnets on a triangular lattice. *J. Phys. C: Solid State Phys.* 19:6825-6831.
- Gu L, Chakraborty B, Garrido PL, Phani M, Lebowitz JL (1996) Monte Carlo study of a compressible Ising antiferromagnet on a triangular lattice. *Phys. Rev. B* 53:11985-11992.
- Terao K (1996) Effect of lattice distortions upon the spin configuration of antiferromagnetic YMn_2 with C15 structure. *J. Phys. Soc. Jpn.* 65:1413-1417.
- Yamashita Y, Ueda K (2000) Spin-driven Jahn-Teller distortion in a pyrochlore system. *Phys. Rev. Lett.* 85:4960-4963.
- Tchernyshyov O, Moessner R, Sondhi SL (2002) Order by distortion and string modes in pyrochlore antiferromagnets. *Phys. Rev. Lett.* 88:067203.
- Schilling T, Pronk S, Mulder B, Frenkel D (2005) Monte Carlo study of hard pentagons. *Phys. Rev. E* 71:036138.
- Villain J, Bidaux R, Carton JP, Conte R (1980) Order as an effect of disorder. *J. Physique* 41:1263-1272.
- Henley CL (1987) Ordering by disorder: Ground-state selection in fcc vector antiferromagnets. *J. Appl. Phys.* 61:3962-3964.
- Henley CL (1989) Ordering due to disorder in a frustrated vector antiferromagnet. *Phys. Rev. Lett.* 62:2056-2059.
- Chubukov A (1992) Order from disorder in a kagome antiferromagnet. *Phys. Rev. Lett.* 69:832-835.
- Reimers JN, Berlinsky AJ (1993) Order by disorder in the classical Heisenberg kagome antiferromagnet. *Phys. Rev. B* 48:9539-9554.
- Bergman D, Alcega J, Gull E, Trebst S, Balents L (2007) Order-by-disorder and spiral spin-liquid in frustrated diamond-lattice antiferromagnets *Nature Physics* 3:487-491.
- Collins MF, Petrenko OA (1997) Triangular antiferromagnets. *Can. J. Phys.* 75:605-655.
- Maignan A, Michel C, Masset AC, Martin C, Raveau B (2000) Single crystal study of the one dimensional $\text{Ca}_3\text{Co}_2\text{O}_6$ compound: five stable configurations for the Ising triangular lattice. *Eur. Phys. J. B* 15:657-663.
- Wang F, Vishwanath A (2008) Spin phonon induced collinear order and magnetization plateaus in triangular and Kagome antiferromagnets: applications to CuFeO_2 . *Phys. Rev. Lett.* 100:077201.
- Starykh OA, Katsura H, Balents L (2010) Extreme sensitivity of a frustrated quantum magnet: Cs_2CuCl_4 . *Phys. Rev. B* 82:014421.
- Wang RF et al. (2006) Artificial 'spin ice' in a geometrically frustrated lattice of nanoscale ferromagnetic islands. *Nature* 439:303-306.
- Han Y et al. (2008) Geometric frustration in buckled colloidal monolayers. *Nature* 456:898-903.
- Chou T, Nelson DR (1993) Buckling instabilities of a confined colloid crystal layer. *Phys. Rev. E* 48:4611-4621.
- Shokef Y, Lubensky TC (2009) Stripes, zigzags, and slow dynamics in buckled hard spheres. *Phys. Rev. Lett.* 102:048303.
- Schmidt M, Löwen H (1996) Freezing between two and three dimensions. *Phys. Rev. Lett.* 76:4552-4555.
- Schmidt M, Löwen H (1997) Phase diagram of hard spheres confined between two parallel plates. *Phys. Rev. E* 55:7228-7241.
- Zangi R, Rice SA (1998) Phase transitions in a quasi-two-dimensional system. *Phys. Rev. E* 58:7529-7544.
- Melby P et al. (2005) The dynamics of thin vibrated granular layers. *J. Phys. Condens. Matter* 17:S2689-S2704.
- Stillinger FH, Salsburg ZW (1967) Elasticity of rigid-disk and -sphere crystals. *J. Chem. Phys.* 46:3962-3975.
- Alder BJ, Hoover WG, Young DA (1968) Studies in molecular dynamics. V. High-density equation of state and entropy for hard disks and spheres. *J. Chem. Phys.* 49:3688-3696.
- Rudd WG, Salsburg ZW, Yu AP, Stillinger FH (1968) Rigid disks and spheres at high densities. III. *J. Chem. Phys.* 49:4857-4863.
- Pusey PN et al. (1989) Structure of crystals of hard colloidal spheres *Phys. Rev. Lett.* 63:2753-2756.
- Woodcock LV (1997) Entropy difference between the face-centred cubic and hexagonal close-packed crystal structures. *Nature* 385:141-143.
- Bolhuis PG, Frenkel D, Mau SC, Huse DA (1997) Entropy difference between crystal phases. *Nature* 388:235-239.
- Woodcock LV (1997) Entropy difference between crystal phases - Reply. *Nature* 388:236-237.
- Mau SC, Huse DA (1999) Stacking entropy of hard-sphere crystals. *Phys. Rev. E* 59:4396-4401.
- Radin C, Sadun L (2005) Structure of the hard sphere solid. *Phys. Rev. Lett.* 94:015502.
- Koch H, Radin C, Sadun L (2005) Most stable structure for hard spheres. *Phys. Rev. E* 72:016708.

39. Ogawa T (1983) A maze-like pattern in a monodisperse latex system and the frustration problem. *J. Phys. Soc. Jpn. Suppl.* 52:167-170.
40. Lynch JM et al. (2010) Glassy dynamics of geometrically frustrated colloidal system. Presented at the APS March Meeting, Portland OR, March 2010. <http://meetings.aps.org/link/BAPS.2010.MAR.D12.11>
41. Tome T, de Oliveira MJ (1990) Dynamic phase transition in the kinetic Ising model under a time-dependent oscillating field. *Phys. Rev. A* 41:4251-4254.
42. Sides SW, Rikvold PA, Novotny MA (1998) Stochastic hysteresis and resonance in a kinetic Ising system. *Phys. Rev. E* 57:6512-6533.
43. Korniss G, White CJ, Rikvold PA, Novotny MA (2000) Dynamic phase transition, universality, and finite-size scaling in the two-dimensional kinetic Ising model in an oscillating field. *Phys. Rev. E* 63:016120.
44. Robb DT et al. (2008) Evidence for a dynamic phase transition in $[\text{Co/Pt}]_3$ magnetic multilayers. *Phys. Rev. B* 78:134422.
45. Sagi E, Ofer O, Keren A, Gardner JS (2005) Quest for frustration driven distortion in $\text{Y}_2\text{Mo}_2\text{O}_7$. *Phys. Rev. Lett.* 94:237202.
46. Rasch JCE et al. (2009) Magnetoelastic coupling in the triangular lattice antiferromagnet CuCrS_2 . *Phys. Rev. B* 80:104431.
47. Ghosh A, Chikkadi VK, Schall P, Kurchan J, Bonn D (2010) Density of States of colloidal glasses *Phys. Rev. Lett.* 104:248305.
48. Chen K, Ellenbroek WG, Zhang Z, Chen DTN, Yunker PJ, Henkes S, Brito C, Dauchot O, van Saarloos W, Liu AJ, Yodh AG (2010) Low-frequency vibrations of soft colloidal glasses *Phys. Rev. Lett.* 105:025501.
49. Kaya D, Green NL, Maloney CE, Islam MF (2010) Normal modes and density of states of disordered colloidal solids *Science* 329:656.
50. Yunker PJ, Chen K, Zhang Z, Yodh AG (2011) Phonon spectra, nearest neighbors, and mechanical stability of disordered colloidal clusters with attractive interactions [arXiv:1103.3535](https://arxiv.org/abs/1103.3535)

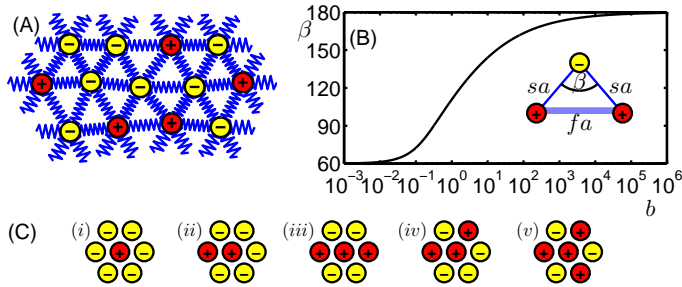


Fig. 1. Model and its ground state: A) Two-dimensional triangular network of antiferromagnetic Ising spins connected with harmonic springs. B) Deformation angle β vs the dimensionless ratio $b \equiv \frac{J\epsilon}{Ka}$ between the magnetoelastic interaction strength and the lattice rigidity, from Eq. (2). Inset: Isosceles triangle with head angle β , satisfied bonds (thin lines) compressed by s and frustrated bond (thick line) stretched by f . C) The five possible configurations (up to rotations and spin inversions) of a particle and its neighbors, with a single frustrated bond in each triangle.

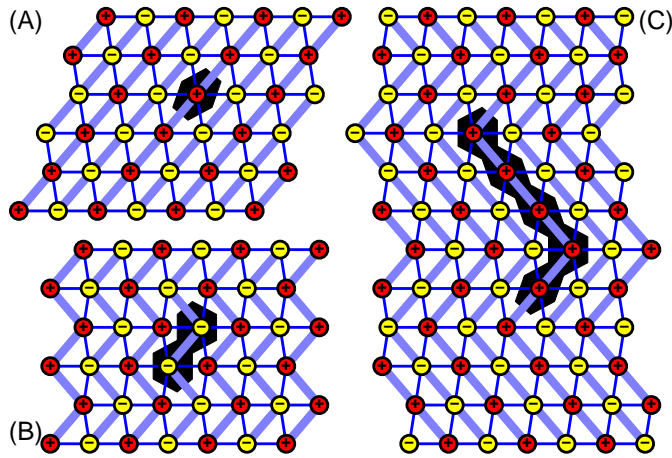


Fig. 2. Zigzagging stripes: Ground-state configurations are generated by stacking layers of particles with alternating spin and with arbitrary relative polarities between successive layers. The figure shows only simple configurations with periodic sequences of the straight (*iii*) and bent (*iv*) segments, as defined in Fig. 1C. However ground-state configurations do not necessarily have a finite unit cell. A) Straight stripes, for which all particles are in the state (*iii*). B) Bent stripes, for which all particles are in state (*iv*). C) Zigzagging stripes with a more complicated unit cell comprised of both (*iii*) and (*iv*). The shaded regions represent the unit cells used for the low-temperature expansion explained in the text. (A), (B), and (C) have one, two and five particles per unit cell, respectively. Thick blue lines represents the stretched frustrated bonds and thin blue lines the compressed bonds for which the antiferromagnetic interaction is satisfied.

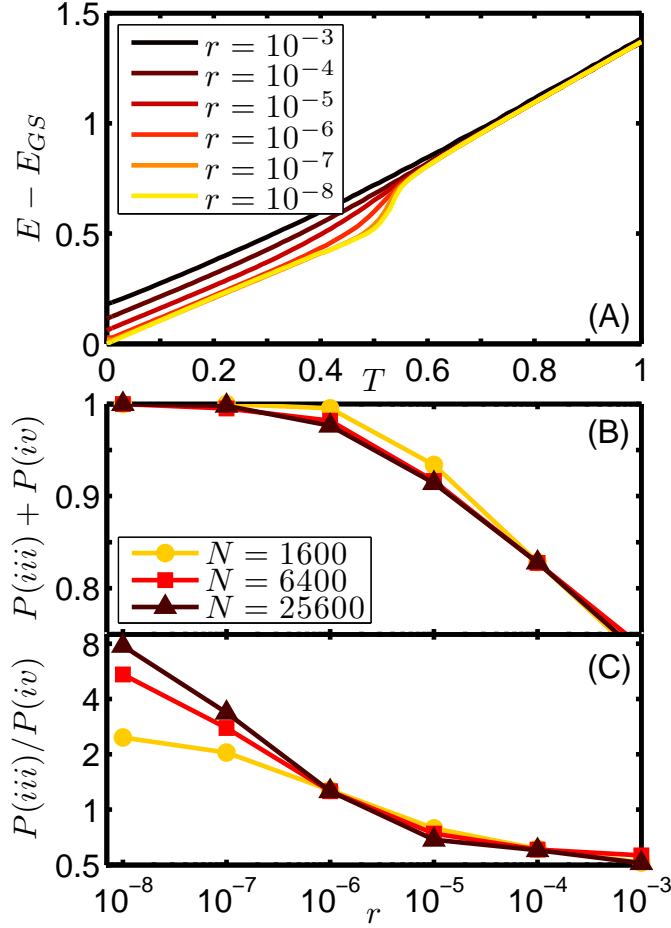


Fig. 3. Monte-Carlo simulations: A) Energy E per particle above the ground-state energy E_{GS} vs temperature T for different cooling rates r as indicated in the legend. System size is $N = 6400$. Similar results were obtained for $N = 1600$ and $N = 25600$. B,C) Probabilities of finding the local configurations (iii) and (iv) defined in Fig. 1C at $T = 0$ following cooling at different rates r for various system sizes N , as indicated in the legend. Note the logarithmic scale for the ratio $P(iii)/P(iv)$ in (C). Error bars are smaller than the symbols. Model parameters in all simulations are $J = 1$, $\epsilon = 2$, $K = 8$, $a = 1$. Thus $b \equiv \frac{J\epsilon}{Ka} = 0.25$. This yields a deformation angle of $\beta = 86^\circ$ in the ground state and a difference in the free-energy coefficient, Eq. (4), of $dA0.05$ between straight and bent stripes.

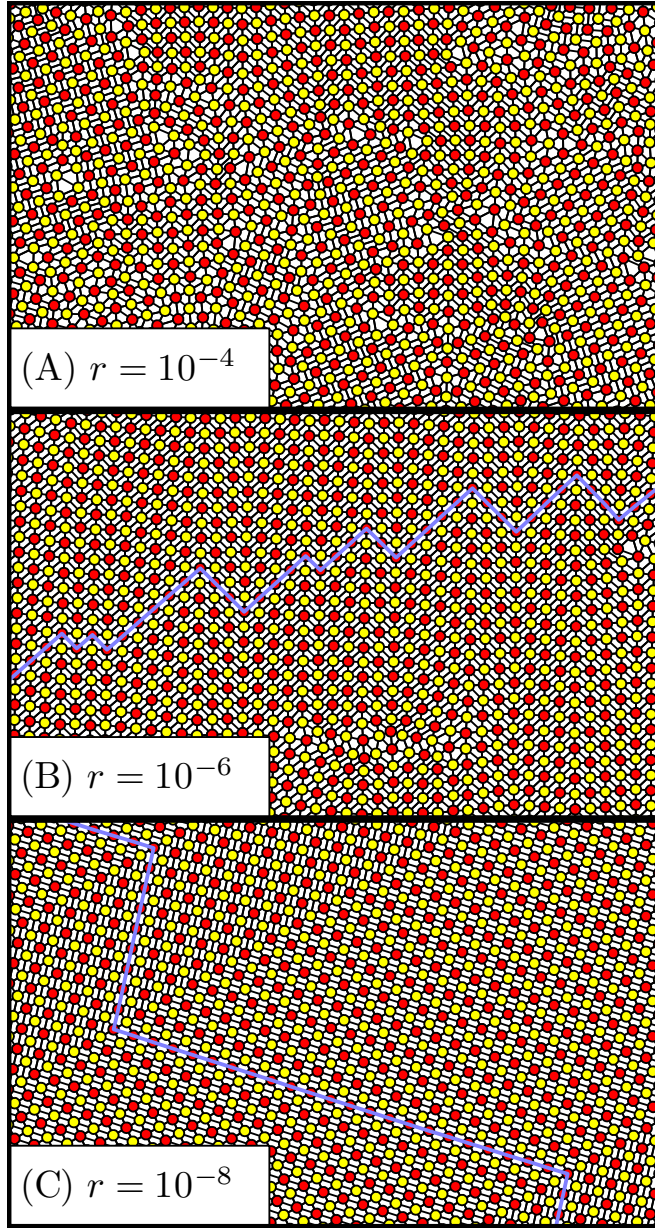


Fig. 4. Ordering with decreasing cooling rate: Portion of the system in its final configuration after cooling at rates $r = 10^{-4}$ (A), 10^{-6} (B), 10^{-8} (C). Model parameters are $J = 1$, $\epsilon = 2$, $K = 8$, $a = 1$. Thus, $b \equiv \frac{J\epsilon}{Ka} = 0.25$, and in the ground state each triangular plaquette is deformed to an isosceles with head angle $\beta = 86^\circ$. System size is $N = 25600$. For the fastest cooling rate, the system falls into a disordered state (A), for which the fraction of particles in the local configuration of a straight stripe (see Fig. 1C) is $P(iii) = 0.31$ and the fraction in that of bends is $P(iv) = 0.52$. For the slower cooling rates, zigzagging stripes are formed (B,C). The blue lines are guides to the eye, which highlight a line of frustrated bonds, and emphasize that as the cooling rate is decreased from (B) to (C), the stripes become more straight. In (B), $P(iii) = 0.54$ and $P(iv) = 0.44$, whereas in (C), $P(iii) = 0.9$ and $P(iv) = 0.1$.

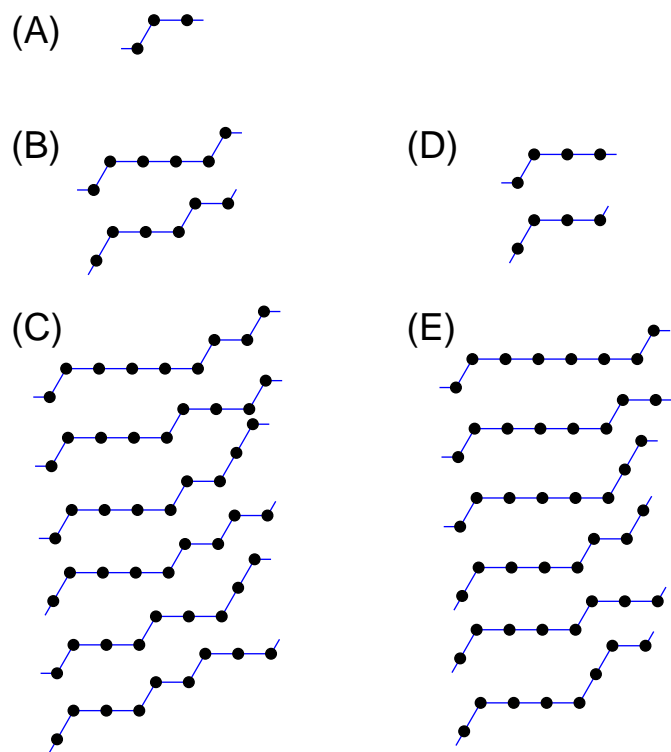


Fig. 5. Examples for some of the unit cells used in evaluating the free energy in Fig. 6: All unit cells with $p_s = 1/3$ containing 3 (A), 6 (B), and 9 (C) particles, and with $p_s = 1/2$ and 4 (D) and 8 (E) particles.

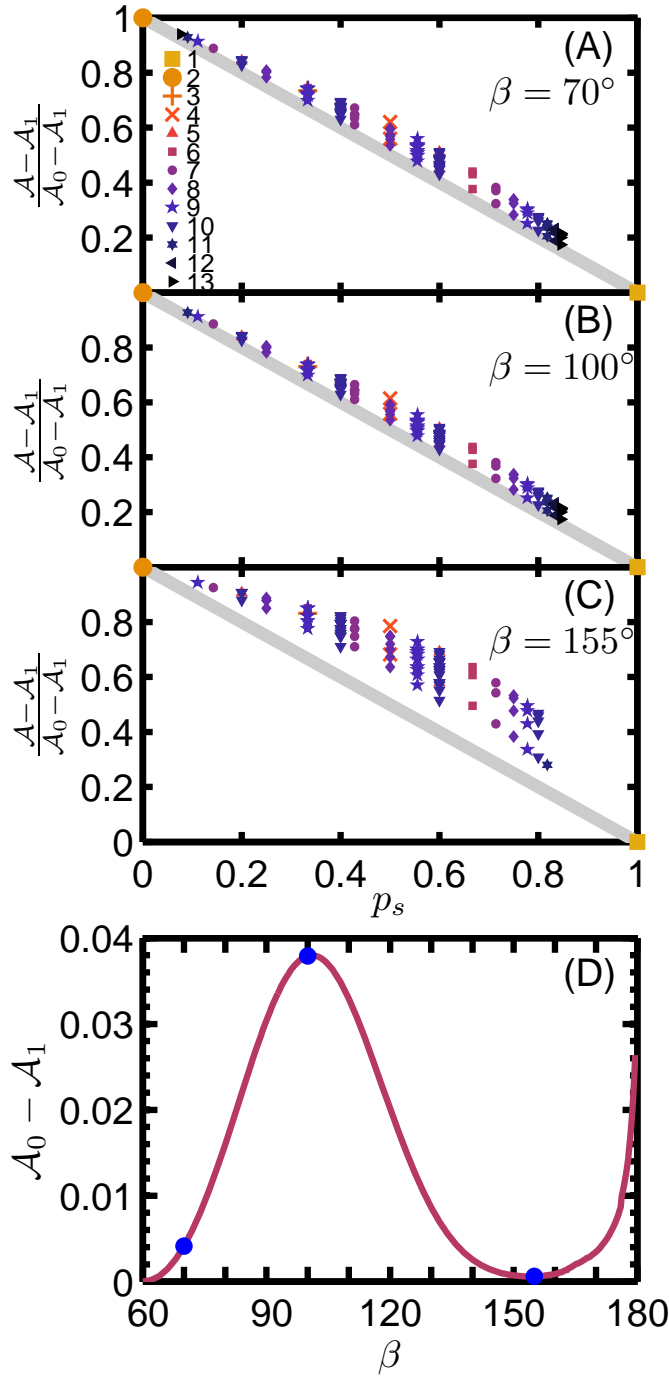


Fig. 6. Normalized entropic contribution, Eq. (4) vs fraction $p_s \equiv P(iii)/[P(iii) + P(iv)]$ of straight-stripe segments for deformation angles $\beta = 70^\circ$ (A), 100° (B), and 155° (C). \mathcal{A} is normalized by its extreme values for straight stripes $\mathcal{A}_1 \equiv \mathcal{A}(p_s = 1)$ and for bent stripes $\mathcal{A}_0 \equiv \mathcal{A}(p_s = 0)$. The gray lines indicate the prediction of a one-dimensional effective Hamiltonian of non-interacting straight and bent segments. The size of the unit cell corresponding to each ground-state configuration is indicated in the legend. We calculated the free energy for all the 95 distinct unit cells consisting of up to 10 particles. Except for straight ($p_s = 1$) and bent ($p_s = 0$) stripes, these have $\frac{1}{9} \leq p_s \leq \frac{4}{5}$. Additionally, of the 363 unit cells with 11-13 particles, we calculated the free energy for 19 unit cells with extreme values of p_s . In numerically evaluating the integration over the Brillouin zone, we require a relative numerical accuracy smaller than 10^{-7} , and therefore for $\beta = 155^\circ$ omitted from the plot 19 unit cells (with 11-13 particles) and for $\beta = 100^\circ$ omitted one unit cell (with 13 particles). See SI Appendix for more details on the calculations and the results. D) Entropic advantage of straight stripes ($p_s = 1$) over zigzags ($p_s = 0$) vs deformation angle. The blue circles indicate the angles for which results for larger unit cells are given in (A-C).